Cryo-electron tomography of the herpesvirus procapsid reveals interactions of the portal with the scaffold and a shift on maturation

Michael H. C. Buch[#], J. Bernard Heymann[#,$], William W. Newcomb[#], Dennis C. Winkler, Alasdair C. Steven

Laboratory of Structural Biology Research, National Institute of Arthritis and Musculoskeletal and Skin Diseases, National Institutes of Health, Bethesda, MD, US.

[#] These authors contributed equally to this study.

[$] Corresponding author. Contact: heymannb@mail.nih.gov

Abstract

Herpes simplex virus type 1 (HSV-1) packages its genome via the portal protein, pUL6, a dodecameric ring at one of the capsid's twelve vertices. While the portal has been visualized in mature capsids, we aimed to describe it in procapsids to elucidate its role in assembly and maturation. Using cryo-electron tomography, we compared procapsids and empty mature capsids (A-capsids) by subtomogram averaging. The portal is located on the interior surface with its narrower end facing outwards in contact with the capsid shell. The portal is embedded in the underlying scaffold, consistent with assembly initiating on a portal-scaffold complex. Maturation involves angularization of the capsid shell, with an accompanying outward movement of the vertices. In A-capsids, the portal translocates further than the surrounding capsomers, enhancing and presumably strengthening its contacts with the capsid shell. We also found a density overlying and offset from the portal vertex corresponding to the expected location of the terminase, the DNA packaging motor.

30 **Introduction**

31 Members of the *Herpesviridae* family cause persistent infections in humans, ranging from cold
32 sores at the lips and genitals to shingles and tumors. While individual members of this family
33 exhibit differences in pathogenicity and structural details, reflected in their classification into
34 three subfamilies, the overall architecture of these viruses is largely conserved. The large genome
35 of HSV-1, the prototypical representative of *Herpesviridae*, is accommodated in a
36 correspondingly massive and complex capsid. During their elaborate life cycle (Mettenleiter,
37 Klupp, & Granzow, 2009), nascent capsids assemble in the nucleus as spherical precursor
38 particles called procapsids (Newcomb et al., 1996; Newcomb et al., 1999; Newcomb et al., 2000),
39 which conform to T=16 quasi-icosahedral symmetry and contain an internal, non-symmetric,
40 spherical scaffold. The scaffold shell consists of the viral proteins pUL26.5 and pUL26, of which
41 the latter is N-terminally fused to a viral protease (Newcomb et al., 2000). Upon completion of
42 the procapsid, the protease is activated and proceeds to cleave the scaffold, initiating maturation
43 of the capsid. Concomitantly, newly completed particles are packaged with viral DNA, a task
44 carried out by a terminase complex (Adelman, Salmon, & Baines, 2001; al-Kobaisi, Rixon,
45 McDougall, & Preston, 1991; Baines, Poon, Rovnak, & Roizman, 1994; Sheaffer et al., 2001;
46 White, Stow, Patel, Hughes, & Preston, 2003; Yu & Weller, 1998). The insertion of DNA and
47 expulsion of scaffold proteins is accompanied by (I) angularization of the capsid; (II)
48 reorganization of the interactions that engage the triplex proteins as well as rearrangement of
49 capsomers (Aksyuk et al., 2015; Heymann et al., 2003; Trus et al., 1996) from skew to more
50 symmetric orientations; (III) conformational changes (Aksyuk et al., 2015; Heymann et al., 2003;
51 Huet et al., 2016; Newcomb et al., 1996; Trus et al., 1996) that establish interactions between
52 capsomer subunits; and (IV) decoration of the mature capsid with additional proteins (Booy et
53 al., 1994; Trus et al., 1995). Maturation increases the capsid's stability dramatically, countering
54 the internal pressure exerted by the tightly packed genome (Bauer, Huffman, Homa, & Evilevitch,
55 2013). This process yields three capsid species, two of which remain in the nucleus. The A-capsid
56 has a mature shell that does not contain any DNA and is essentially empty, while B-capsids retain
57 a shrunken and somewhat disordered scaffold despite having matured into an angular shape.
58 Only mature, DNA-filled capsids, called C-capsids, leave the nucleus and do so via the perinuclear

space (reviewed in (Johnson & Baines, 2011; Mettenleiter, Muller, Granzow, & Klupp, 2013)), to undergo the subsequent steps in the viral life cycle.

Terminase association with the procapsid and DNA insertion occur at a single fivefold vertex of the particle, which is occupied by a portal complex formed by the protein pUL6 (Newcomb et al., 2001) and replaces a penton of the major capsid protein, pUL19. Early structural investigations (Trus et al., 2004) revealed the portal to be a dodecameric ring strikingly similar to structures found in bacteriophages. In the following years, placement and orientation of this complex in the context of the capsid have remained elusive. Investigations by cryo electron microscopy (cryo-EM) were hampered by the fact that the portal accounts for only about 1% of the capsid protein mass. In addition, unlike in bacteriophages, the vertex housing the portal does not feature a tail structure and thus is difficult to distinguish in electron micrographs from non-portal-bearing vertices. A variety of imaging methods were employed, but uncertainty persisted regarding placement of the portal (Cardone et al., 2007; Rochat et al., 2011; Schmid et al., 2012). This changed recently, when technological advances in cryo-EM enabled high-resolution reconstructions of portal-bearing vertices in mature capsids for several herpesviruses (Gong et al., 2019; Liu, Jih, Dai, Bi, & Zhou, 2019; McElwee, Vijayakrishnan, Rixon, & Bhella, 2018; Wang et al., 2020). The structures of these end-point assemblies, however, provide limited insight into the assembly and maturation of capsids in the absence of information on immature particles.

In this study, we have pursued an alternative approach to identifying the portal-related density in an otherwise symmetric particle – cryo-electron tomography (cryo-ET), coupled with sensitive particle processing. As a control, we imaged A-capsids, and located the portal on the inside of the particle with its wider portion facing inwards. We then examined procapsids and found that the portal engages in abundant contacts with the scaffolding layer. Our reconstructions also show faint density above the portal-bearing vertex that is consistent with the expected location of the terminase.

88 **Results**

89 **Identification of the portal vertex in cryo-electron tomograms.** Our aim was to locate the portal
90 using cryo-ET to clarify its position during maturation. Tomography has the advantage over single
91 particle analysis (SPA) of allowing the extraction of 3D particles rather than 2D projections, which
92 renders the identification of unique features straightforward. Expanding on an earlier
93 tomographic protocol (Cardone et al., 2007), we added a new program called bico to the existing
94 Bsoft package (Heymann, Cardone, Winkler, & Steven, 2008). An overview of our workflow is
95 given in Fig. S1. From reconstructed tomograms, randomly oriented 3D particles are extracted
96 and aligned to an icosahedral reference, in our case a reconstruction of a HSV-1 C-capsid
97 (accession number EMDB-7472 (Dai & Zhou, 2018)). Next, the fivefold vertices of each capsid are
98 extracted, and an average of all extracted and correctly oriented vertices is calculated. For each
99 set of 12 vertices, bico then compares a masked region in each vertex with this average and,
100 based on masked cross-correlation, classifies each vertex set into two subsets: the first subset
101 contains the eleven best-fitting vertices. These vertices will have a high score, because they house
102 pentons and are therefore closely similar to the average of all vertices. The second subset
103 contains the vertex with the worst fit, taken to be the portal vertex. The coordinates of the
104 identified portal vertices are then transferred back into the extracted and aligned capsids, and a
105 reconstruction of the capsid featuring the portal vertex is calculated. To reduce noise, this
106 reconstruction is symmetrized fivefold in the final step.

107

108 **Production of capsid samples using a pUL25-deficient mutant.** As a first step, we decided to
109 analyze mature A-capsids to avoid interference from internal density features such as scaffolding
110 (cf. B-capsids) or packaged DNA (cf. C-capsids). The established protocol for purifying HSV-1
111 nucleocapsids from a wild-type infection yields a minor fraction of A-capsids. To increase their
112 yield, we used a mutant lacking the vertex protein, pUL25, that is defective in DNA packaging
113 (McNab et al., 1998). This virus replicates in a complementary African Green Monkey cell line
114 transfected with the UL25 gene, but in wild-type cells cannot produce progeny. In our protocol,
115 analytical ultracentrifugation on small-scale gradients yielded bands for A-capsids and B-capsids
116 but no band for the DNA-filled C-capsids (Fig. 1A). We isolated the A-capsid band (hereafter called

UL25-Null A-capsids) and collected tilt series for cryo-ET. Individual capsids were well spread out in the sample, and almost all capsids could be confirmed as A-capsids from their empty appearance (Fig. 1B). From these data, we were able to extract a total of 176 UL25-Null A-capsids.

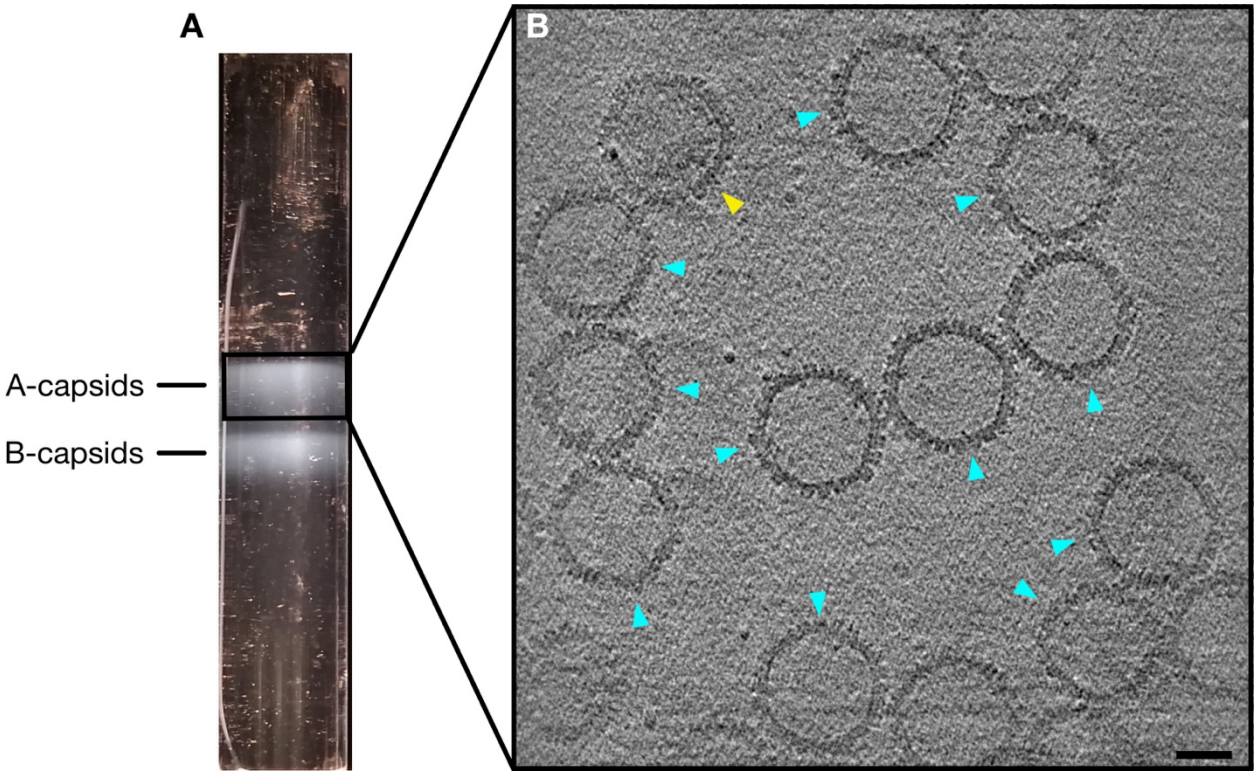

Fig. 1. Preparation of UL25-Null A-capsids. **A.** Analytical small-scale sucrose gradient of capsid mix obtained during initial purification. Bands of A- and B-capsids are labeled. **B.** Central slice of a typical tomographic reconstruction for UL25-Null A-capsids. The individual particles are well defined and separated (turquoise arrowheads). Occasionally, a capsid with some internal content – probably some scaffold – were found in the field of view (yellow arrowhead). These particles were not included in further processing. Scale bar, 500 Å.

The portal-bearing vertex of UL25-Null A-capsids. We identified the portal-bearing vertex on each of these UL25-Null A-capsids and calculated a reconstruction in the context of the capsid (Fig. 2). In line with recent publications (Liu et al., 2019; McElwee et al., 2018; Wang et al., 2020), we located the portal on the inside of the capsid, with its wider end facing towards the center of

134 the particle (Fig. 2A). A superposed atomic model of the HSV-1 portal (PBD ID 6OD7 (Liu et al.,
135 2019)) fits into the portal density (Fig. 2B). The portal has a narrow end called the "clip domain"
136 that engages the triplexes (green arrow in Fig. 2B) and lines the DNA translocation channel. The
137 widest part of the portal, the "wing domain" extends towards floor of the neighboring capsomers
138 (blue arrow in Fig. 2B). The overall appearance and placement of this connection is consistent
139 with a set of β-barrels and spine helices originating from the pUL19 hexons that were identified
140 earlier in a high-resolution reconstruction (Liu et al., 2019). Knowing what it looks like, we could
141 identify the portal vertex in individual particles in our tomograms (white arrows in Fig. 2C).
142
143 Moreover, we have observed an additional density offset from the outside of the capsid, which
144 we judge to be too strong to be symmetrized noise (orange arrow in Fig. 2B). This location is
145 consistent with expectations for the terminase complex, although this density is smaller than in
146 a recently reported reconstruction (100 Å x 100 Å vs. 225 Å x 100 Å (Y. Yang et al., 2020)). We
147 expect only residual terminase to be present on UL25-Null A-capsids, because A-capsids have
148 been reported to retain little of this protein (Sheaffer et al., 2001), and the absence of pUL25 in
149 our capsids may exacerbate this deficiency. In addition, it has been reported that the terminase
150 makes contact with capsids (Sheaffer et al., 2001; Yu & Weller, 1998), particularly through pUL6
151 (White et al., 2003).
152

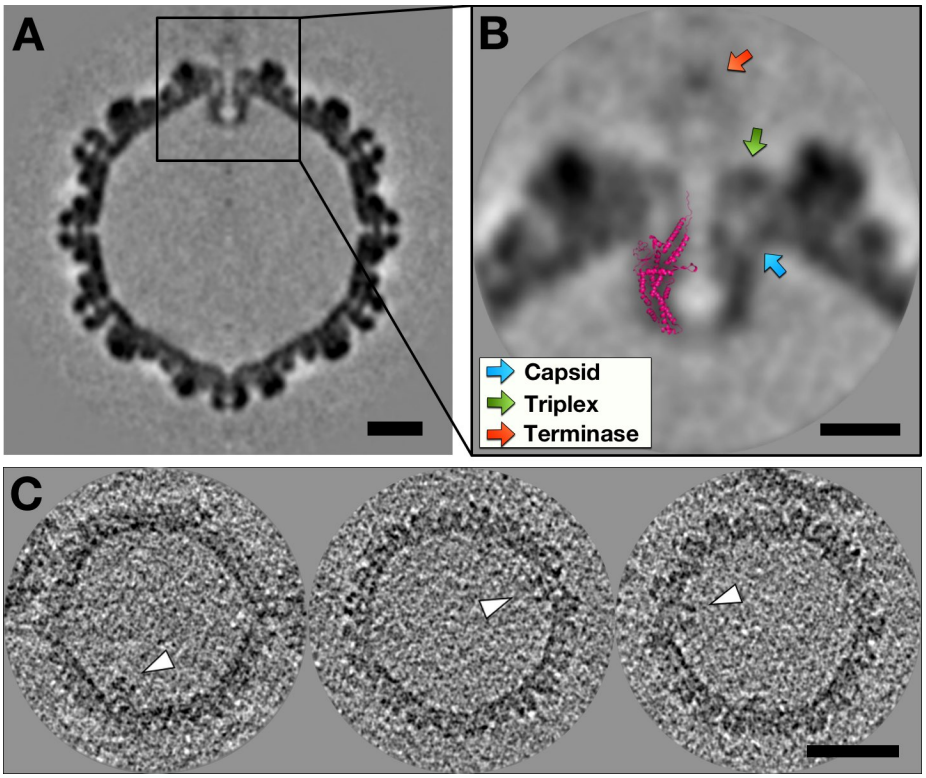

Fig. 2. The portal vertex in UL25-Null A-capsids. A. Central slice of the C5-symmetrized capsid with the portal vertex located at the top. Scale bar, 200 Å. **B.** Magnified view of the vertex. The portal is located beneath the capsid floor with its wider end facing the inside of the particle. A high-resolution model (pink, PDB ID 6OD7 (Liu et al., 2019)) is superimposed on the left half of the portal density. The portal forms connections to the triplex (green arrow) and the capsid floor (blue arrow). We also observe a faint but definitely present density overlying the vertex measuring 100 Å at its widest point and 100 Å in height (orange arrow). Scale bar, 100 Å. **C.** Slices from tomograms of UL25-Null A-capsids that traverse the portal in each (white arrowheads). Scale bar, 500 Å.

The portal in procapsids interacts with the scaffold. Procapsids were produced using the M100 mutant that lacks the viral protease VP24 required for rapid maturation (Gao et al., 1994). We followed a gentle purification protocol (Aksyuk et al., 2015) to avoid damage to the particles. For a successful identification of the portal vertex in procapsids, several precautions were taken: since procapsids are fragile and malleable, we used an antibody binding to the major capsid

170 protein (Newcomb et al., 1996) that stabilized the particles. For processing, we selected well-
171 separated spherical particles (Fig. S2), and we acquired a larger number of particles: 368. The
172 analysis relies on a mask to isolate the portal density from the rest – we were careful to adjust
173 the mask so that it excluded the scaffold, which might otherwise outweigh the portal density
174 during vertex sorting. This procedure allowed us to identify the portal vertex in procapsids
175 (Fig. 3). As with UL25-Null A-capsids, the portal is oriented towards the inside of the particle (Fig.
176 3A), again consistent with an atomic portal model (Fig. 3B). The portal penetrates deeply into the
177 scaffold layer (yellow arrow in Fig. 3B), almost to the widest part of its wing, a position that allows
178 the formation of extensive interactions. Interestingly, the nominally spherical scaffold shows a
179 degree of perturbation caused by the portal, giving the scaffold an overall teardrop shape
180 (Fig. 3A). We also note that – apart from in the portal region - the scaffold shell shows up in slices
181 as three concentric rings (arrows in Fig. 3A) and conclude that the scaffold protein pUL26.5 is an
182 elongated molecule consisting of three domains plus a thin linker not visualized here that
183 connects it to the capsid shell. Only tenuous contacts (blue arrow in Fig. 3B) are formed between
184 the portal and the surrounding hexons, but the wing domain appears to interact with the
185 triplexes (green arrow in Fig. 3B). The vertex overall has a funnel-like shape that likely
186 accommodates DNA insertion by the terminase complex. As with the A-capsid, we detect a
187 density overlying the vertex (orange arrow in Fig. 3B), albeit much fainter in this case, despite an
188 earlier report that isolated procapsids contain more of the terminase than A-capsids (Sheaffer et
189 al., 2001). Indeed, it makes sense that this complex should mostly occupy procapsids in order to
190 fill them with viral DNA. Finally, the procapsid hexons also display faint residual density on their
191 exterior parts (Fig. 4B; see also faint density decorating capsomers in Fig. 3A) that we attribute
192 to the 6F10 antibody used to stabilize the procapsids during isolation (see Methodology)).
193

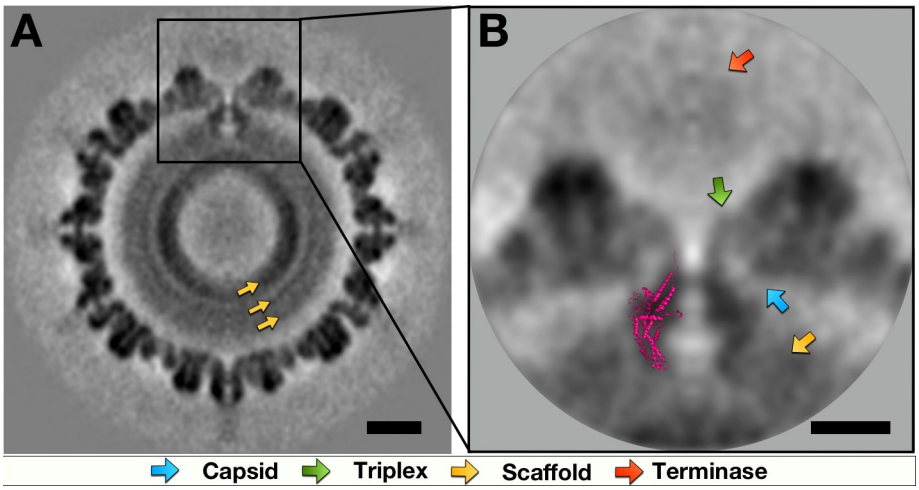

Fig. 3. The portal vertex in procapsids. A. Central slice of the C5-symmetrized procapsid with the portal vertex at the top and showing distinct rings of scaffold density (yellow arrows). Scale bar, 200 Å. **B.** Magnified view of the portal vertex with a superimposed atomic model (pink, PDB ID 6OD7 (Liu et al., 2019)). The portal is mainly connected to the capsid through the triplex (green arrow) with a thin connection to the capsid floor (blue arrow). The bottom of the portal is embedded in the scaffold (yellow arrow). As in UL25-Null A-capsids (Figure 2), we observe a faint density over the portal vertex (orange arrow). Scale bar, 100 Å.

Conformational changes and movement of the portal during maturation. While the portal orientation is similar in procapsids and UL25-Null A-capsids, contrasts in vertex configuration come to light in a side-by-side comparison (Fig. 4A). Upon maturation, the capsid becomes angular, causing the vertex itself to jut out. This movement involves an outward shift of about 32 Å for the hexons, as well as the angles between the capsid line and the fivefold vertex becoming more acute. We also notice a strongly defined, linear density on the bottom of the UL25-Null A-capsid shell, which is most likely the established capsid floor that conveys capsid stability (Huet et al., 2016) (see also Fig. 2B). Strikingly, while the capsomers move by about 32 Å, the portal itself shifts axially by about 61 Å (Fig. 4A). This increment of about 30 Å is accompanied by an establishment of contacts with the capsid floor, as described above.

We also observe a shift in the triplex network surrounding the portal vertex, which narrows the vertex channel. These changes become even more apparent when the vertices are viewed from the top (Fig. 4B). While triplexes are somewhat weakly defined in the procapsid portal vertex, they become much more visible in the UL25-Null A-capsid and even extend towards the fivefold symmetry axis. It is possible that some of this extending density could be ascribed to components of the tegument, particularly pUL17. We recall that, upon maturation, the hexons rearrange from a skewed orientation to true hexameric symmetry (Aksyuk et al., 2015).

We also compared the triplexes of the portal vertex with those of the opposing penton vertex in both maps. The triplexes in the procapsid portal vertex are poorly defined (Fig. 5A) making it hard to ascertain whether they are in the same orientation as those at the opposing penton vertex (Fig. 5B). In contrast, the orientation of the triplexes is clearly the same for both vertices in the UL25-Null A-capsid (Fig. 5C,D).

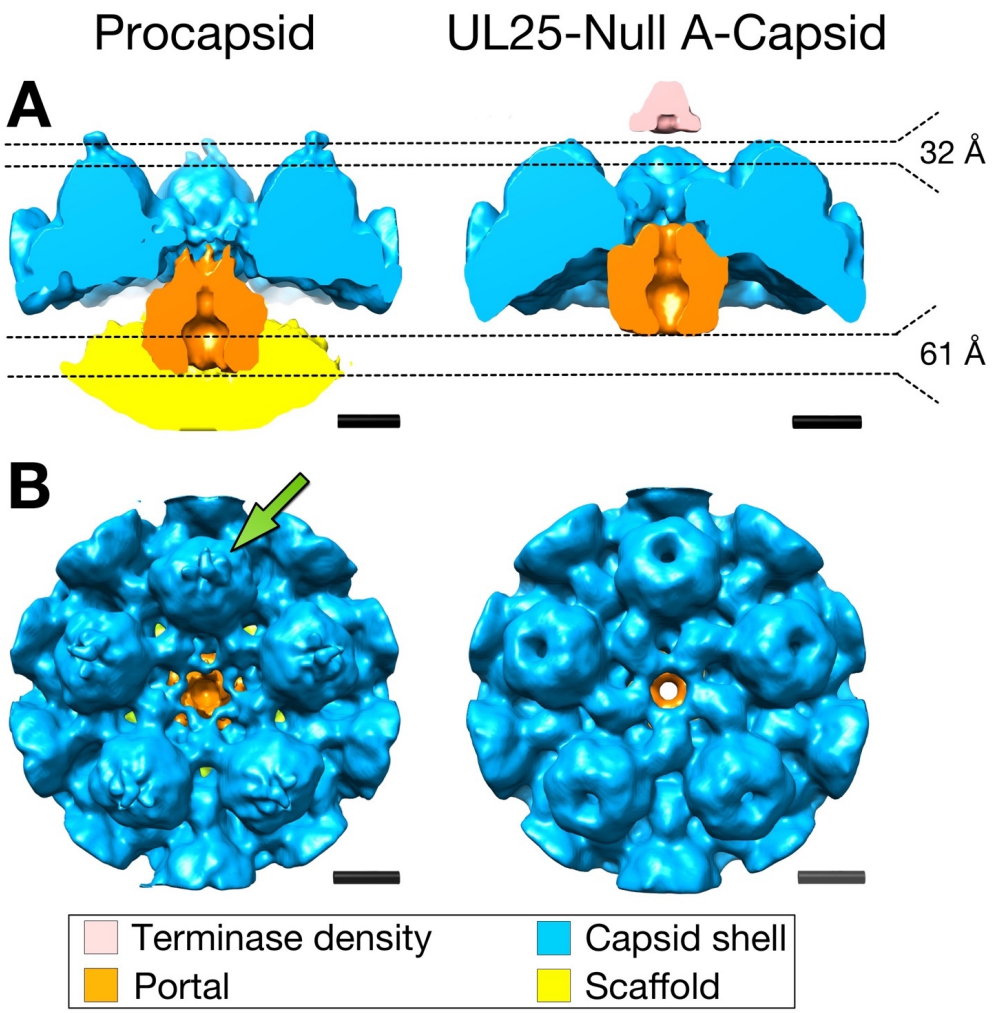

Fig. 4. Comparison of portal vertices in procapsid and UL25-Null A-capsid. A. Segmented isosurface renderings of the two vertices, reconstructed at the same distance from their capsid centers. Angularization during maturation translocates the hexons surrounding the vertex by ~32 Å, while the portal shifts ~61 Å, tightening its interactions with the surrounding capsomers. **B.** Top view comparisons of the isosurface renderings (offset portal densities omitted for clarity). The portals themselves (orange) face away from the viewer. Upon maturation, the triplex networks surrounding the vertex shift and constrict the vertex channel, and the hexons transform from skewed ovals towards hexagonal symmetry. The faint extraneous density associated with the hexons can be attributed to the 6F10 antibody used in the preparation of the particles (green arrow). Scale bars, 100 Å.

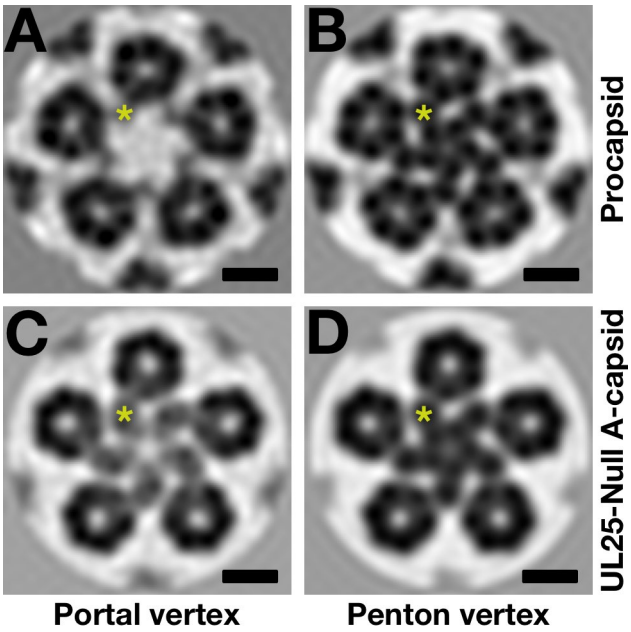

Fig. 5. The arrangement of triplexes at the vertices. The triplexes (yellow stars) at the procapsid portal vertex (**A**) are recessed relative to those at the opposite penton vertex (**B**) (slices at a radius of 307 Å). In contrast, the triplexes at the UL25 Null A-capsid portal vertex (**C**) are closer to conformation of those at the opposite penton vertex (**D**) (slices at a radius of 325 Å). Note that the vertices in the procapsid move outwards by ~20 Å on maturation, accounting for the differences in slices shown here. Scale bars, 100 Å.

Discussion

Localization and interactions of the portal in A-capsids and procapsids. In a critical step of the HSV-1 life cycle, newly synthesized DNA is fed into the capsid which undergoes extensive conformational changes as it matures (Aksyuk et al., 2015; Heymann et al., 2003) although this process can occur without DNA packaging (Heymann et al., 2003) and may precede DNA packaging *in vivo* (Church & Wilson, 1997). In both herpesviruses and tailed bacteriophages, DNA is inserted through a single fivefold vertex via the dodecameric portal protein. While the overall structure of the HSV-1 portal, pUL6, has been known for some time (Trus et al., 2004), its orientation and placement in the context of the capsid shell have been subject to debate. The portal's overall shape makes it difficult to distinguish visually from capsomer pentons in

261 micrographs, making consistent alignment of 2D projections a challenge. In an earlier study, we
262 used cryo-ET, aiming to characterize the portal vertex of HSV-1 (Cardone et al., 2007). Here, we
263 have refined this approach by developing a new program designed to identify the portal vertex
264 on individual capsids, thereby allowing coherent averaging. Applying it to HSV-1 A-capsids, we
265 located the portal on the inside of the particle, consistent with several recent SPA-based studies
266 (Gong et al., 2019; Liu et al., 2019; McElwee et al., 2018; Wang et al., 2020). In confirmation, an
267 atomic model of pUL6 (Liu et al., 2019) fits well into our portal density (Fig. 6). This density
268 extends beyond the clip domain of the model, presumably representing some of residues 308-
269 515 not modeled (corresponding residues are also unmodeled in a reconstruction of the Epstein-
270 Barr-virus portal (Machon et al., 2019)). Interestingly, a corresponding turret-shaped density was
271 discovered in the portal vertex of Kaposi's Sarcoma Herpesvirus (KSHV) (Gong et al., 2019); it was
272 theorized that this helical turret is an extension of the portal's clip domain and could be a docking
273 site for the terminase complex. We do not observe any funnel-like arrangement of α-helices that
274 was described in HSV-1 virion capsids (Liu et al., 2019; McElwee et al., 2018). If such a component
275 is indeed an additional protein, it may only be added to mature particles upon the successful
276 retention of DNA.
277

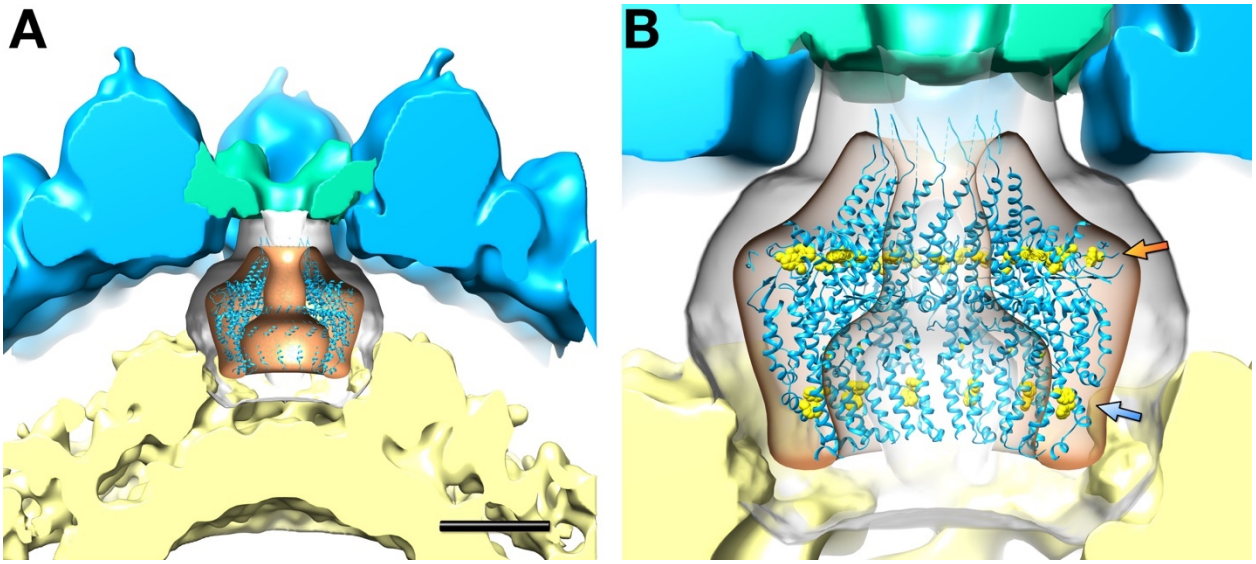

278
279 **Fig 6**. **The model of the portal within the context of the procapsid portal vertex. A.** The portal
280 model (PDB ID 6OD7 (Liu et al., 2019)) fitted into the portal density (orange) within a lower

281 threshold envelope (grey) to show the connections to the triplexes (green) and the scaffold
282 (yellow). The connections to the capsid shell (blue) are not resolved in this map. Scale bar, 100
283 Å. **B.** Close-up view of the portal with key tryptophan residues (yellow) at the wing (orange
284 arrow: W163, W241, W262, W532) and at the bottom (blue arrow: W90, W127) that were
285 shown to interact with the scaffold (K. Yang & Baines, 2009b).
286
287 Applying our workflow to procapsids revealed several novel observations. The procapsid portal
288 is located inside the vertex forming contacts with the scaffolding shell and disrupts the scaffold
289 proteins' spherical arrangement at the interaction site. Conserved tryptophan residues have
290 been identified in HSV-1 pUL6 ((K. Yang & Baines, 2009b), see also Fig. 2 in (Dedeo, Cingolani, &
291 Teschke, 2019)) that play crucial roles in interaction between portal and, most likely, conserved
292 pUL26.5 residues 143-151, particularly YYPGE (Singer, Newcomb, Thomsen, Homa, & Brown,
293 2005; K. Yang & Baines, 2009a). Figure 6B shows these critical tryptophan residues locate in the
294 wing domain as well as towards the bottom. We know the scaffold C-terminus is bound to the
295 capsid which puts it in the proximity of the portal wing domain. Conserved tryptophan residues
296 are a feature not only of HSV-1 but also of some bacteriophages ((Guasch et al., 2002), reviewed
297 in (Dedeo et al., 2019)). The extensive and presumably strong interactions observed here support
298 the hypothesis that a complex of portal plus scaffolding protein serves as the nucleation point
299 for procapsid assembly, to be followed by the addition of protomers, each consisting of a triplex
300 surrounded by three copies of the major capsid protein with three scaffolding protein dimers
301 (Aksyuk et al., 2015). The scaffold presumably shares the symmetry of the surface shell with
302 which it co-assembles but is not highly ordered and its sphericity is enhanced by averaging. In it,
303 we see three concentric shells (Fig. 3), consistent with a previously observed structure and model
304 of a scaffold dimer (see Fig. 6B in (Aksyuk et al., 2015)).
305
306 **The portal shifts axially upon particle maturation.** One noteworthy finding from comparing the
307 portal vertices of UL25-Null A-capsids and procapsids is the axial shift of the portal upon
308 maturation. Angularization of the maturing capsid causes the entire vertex to shift by ~32 Å and
309 the portal by ~61 Å. This movement is accompanied by the establishment of a support network

310 with the newly established capsid floor (termed suspension network in an earlier study (Liu et al.,
311 2019)). While we did not analyze C-capsids, we suspect that DNA packaging, a process that
312 generates substantial internal pressure in the capsid may push the portal outwards enabling the
313 establishment of the portal suspension network and making it "click" into a more stable
314 configuration, which, in turn, may also play a role in releasing viral DNA into the nucleus as the
315 virus infects a new cell. Of note, an axial shift of the portal has also been observed in HSV-2,
316 where B-capsids were compared to virion capsids (Wang et al., 2020). Although equating HSV-1
317 and HSV-2 warrants caution, this movement is consistent with our observations.
318
319 **Morphological changes of the particle upon maturation.** The overall shape of the portal vertex
320 differs significantly between procapsids and mature capsids (Fig. 4). In procapsids, we note that
321 the center of the vertex is essentially open, which would, in a biological context, be advantageous
322 for the insertion of DNA. Triplex density is present around the portal vertex, but it is somewhat
323 fainter than around a penton vertex, which could result from a lack of interaction between the
324 portal and the procapsid itself. In the mature capsid, the vertex is narrower, and it appears that
325 density originating at the triplexes extends towards the vertex axis. This extended density may
326 indeed be contributed by components of the tegument, particularly pUL17. While our A-capsids
327 lack pUL25, it has been shown that procapsids contain practically no pUL25 (Sheaffer et al., 2001),
328 and given that the procapsid undergoes substantial conformational changes during maturation,
329 it is likely that no tegument component protein is present on these immature particles. The
330 extended, star-shaped density we see on the UL25-Null A-capsid portal vertex (Fig. 4B) may
331 therefore act as a docking platform for copies of pUL25 that would be added in the course of a
332 wild type infection and α-helices contributed by pUL36 at a later stage. This platform, however,
333 is evidently insufficient to retain DNA in the capsid, as the absence of pUL25 alone is enough to
334 completely prevent the emergence of propagation-competent, DNA-filled C-capsids (McNab et
335 al., 1998), underscoring pUL25's functional versatility as a DNA retention protein and a key player
336 in nuclear egress as well (Draganova, Zhang, Zhou, & Heldwein, 2020).
337

338 **Presence of putative terminase density at the portal vertices.** Our reconstructions revealed faint
339 density offset from the portal vertex. We originally observed this density associated with UL25-
340 Null A-capsids, prompting us to suspect that it may be ascribed to the terminase complex. This
341 complex has been found to still be associated with A-capsids in relatively low amounts (Sheaffer
342 et al., 2001), but the dimensions we could measure at our resolution are at odds with a recently
343 reported reconstruction of the complex (Y. Yang et al., 2020). This could be due to A-capsids
344 carrying only residual terminase density and that part of the complex was sheared off in the
345 preparation process of our UL25-Null A-capsids. The absence of pUL25 may have further
346 contributed to reduced terminase presence. This putative terminase density was only very faintly
347 present in procapsids, even though they should display a stronger occupancy than any other
348 capsid type (Sheaffer et al., 2001). Our preparation protocol (Aksyuk et al., 2015) involves
349 numerous filtration steps that may have detached the terminase from many procapsids.
350 Additional experiments such as antibody labeling are needed to confirm the identity of this
351 density, but its location is consistent with where we would expect terminase to dock onto the
352 procapsid. At this location, the complex would have easy access to the outermost parts of the
353 portal's clip domain to form interactions (White et al., 2003), and the funnel-like overall shape of
354 the procapsid's portal vertex shown here could easily accommodate the insertion of DNA, while
355 the narrower topography of the mature capsid's vertex could facilitate rapid genome ejection.
356 In conclusion, our routine for processing cryo electron tomograms enabled us to visualize the
357 portal in mature HSV-1 capsids and in procapsids, revealing not only interactions of scaffold with
358 the portal but also rearrangement of the portal vertex upon maturation. We also gained insights
359 into the intricate maturation-induced changes in the portal vertex.
360

361 **Material and Methods**

362 **Cell handling and propagation of virus stocks.** Stocks of the UL25 deletion mutant (UL25-null)
363 (McNab et al., 1998) were generated by using a complementary African Green Monkey cell line
364 (both gifts from Prof. Fred L. Homa, University of Pittsburgh, Pittsburgh, PA). At roughly 75%
365 confluency, monolayers in 175 cm^2 flasks were infected with virus stock at a MOI of 0.1 in 1 mL
366 of PBS without calcium or magnesium per flask for 40 min at room temperature, followed by 5

367 min at 37˚C. The cells were then overlaid with 15 mL virus growth medium (1x MEM Alpha,
368 Corning, 1.5% (*v/v*) penicillin/streptomycin) and incubated at 37˚C. At 48 h post infection, virus-
369 containing medium was clarified by centrifugation at 1,500 rpm for 5 min, and crude cell debris
370 was removed from the supernatant by pelleting at 6,000 rpm for 15 min in a Beckman SW28
371 rotor. Virus was pelleted for 45 min at 19,000 rpm in a Beckman SW28 rotor. The virus pellets
372 were resuspended in small volumes of PBS without calcium or magnesium, and aliquots of 500
373 µL were frozen at -80˚C. The virus titer was assessed in complementary cells 48 hr. after infection.
374 Stocks of the procapsid-producing M100 line (Gao et al., 1994) were generated similarly using
375 the complementary F-3 cell line. Stock titers were assessed as described earlier (Aksyuk et al.,
376 2015).
377 **Production of capsids.** Roller bottles of African Green Monkey cells were grown to about 75%
378 confluency and infected with UL25-null virus stocks at a MOI of 10. 14 hr post infection, cells had
379 started to round up, but not detach from the surface. Cells were harvested by centrifugation at
380 1,500 rpm for 5 min, and any virus still attached to the cell surface was removed by incubation
381 with TNE (20 mM Tris, pH 7.4, 500 mM NaCl, 1 mM EDTA) on ice for 15 min. Cells were again
382 pelleted for 5 min at 2,000 rpm, resuspended in TNE, and broken up by sonication. 1.5% (*v/v*)
383 TX-100 was added to solubilize nuclear membranes, followed by pelleting of crude cell debris for
384 30 min at 6,000 rpm in a Beckman SW28 rotor. The resulting supernatant was supplemented with
385 a cushion of 30% (*w/v*) sucrose in TNE, and a mix of A- and B-capsids was pelleted for 1 h at
386 20,000 rpm in a Beckman SW28 rotor. The pellets were resuspended in TNE, supplemented with
387 complete protease inhibitor cocktail (Roche), and applied to a preparative gradient containing a
388 range of 20-50% (*w/v*) sucrose in TNE. The gradient was run for 1 h at 22,000 rpm in a Beckman
389 SW55Ti rotor. Distinct bands containing the different capsid species were isolated, pelleted for
390 50 min at 22,000 rpm in a Beckman SW55Ti rotor, and resuspended in small amounts of TNE to
391 reach an appropriate concentration for cryo-ET.
392 Procapsids were produced as described earlier (Aksyuk et al., 2015). They were precipitated with
393 an antibody reacting to pUL19 for purification and capsid stability purposes (Newcomb et al.,
394 2000).

395 **Grid preparation and cryo-electron tomography.** Procapsids stabilized by the pUL19 antibody
396 and UL25-null A-capsids were mixed with Aurion Anionic 10 nm BSA gold tracers (EMS) at a 1:1
397 ratio, and 3 µL were applied to Quantifoil copper grids covered with 300-mesh holey carbon
398 (EMS), which were previously plasma-cleaned for 12 s with an argon-oxygen mixture (25%
399 oxygen) in a Model 1020 plasma cleaner (Fischione, Export, PA). Using a Leica EM GP
400 plunger (Leica Microsystems Inc., Buffalo Grove, IL), excess liquid was blotted off for 2.5 s, and
401 grids were flash-frozen in liquid ethane. For the UL25-null A-capsids, 21 tilt series ranging from -
402 57˚ to +57˚ at 3˚ increments were collected at 20,000 x magnification and a defocus target of -
403 2.5 µm on a JEOL JEM-2200FS cryo-electron microscope operating at 200 kV and equipped with
404 an in-column energy filter and a K2 Summit detector (Gatan, Warrendale, PA). For procapsids, 80
405 tilt series ranging from -57˚ to +57˚ at 3˚ increments at 81,000x magnification and a -2 µm defocus
406 target were acquired on a 300 kV Titan Krios (Thermo Scientific, FEI, Hillsboro, OR) equipped with
407 a post-column Model 967 GIF Quantum-LS with a K2 Summit detector (Gatan, Warrendale, PA).
408 In both cases, data were acquired using SerialEM (Mastronarde, 2005).
409 **Tomogram reconstruction and identification of the portal-bearing vertex.** Image processing and
410 tomogram reconstruction were carried out using Bsoft (Heymann et al., 2008). Tomograms were
411 binned 2-fold, resulting in a final pixel size of 3.66 Å for UL25-null A-capsids and 3.61 Å for
412 procapsids. For both capsids, promising particles were extracted in 450 x 450 x 450 pixel boxes
413 and aligned to a reference of a HSV-1 C-capsid (Dai & Zhou, 2018). 12 vertices per capsid were
414 extracted in 150 x 150 x 150 pixel boxes centered 140 pixels outward from the center of the
415 particle on the fivefold symmetry axes. Using the new Bsoft program, bico, for each set of 12
416 vertices, the masked cross-correlation against an average calculated from all vertices was
417 calculated, and the vertex with the lowest correlation was deemed the portal-bearing vertex. To
418 address the symmetry mismatch between the fivefold vertex and the twelvefold portal, the best
419 orientation of the portal-bearing vertices was found and refined using bico, followed by
420 transferring the coordinates of the portal-bearing vertices back into the extracted capsids. From
421 this, reconstructions of the whole capsids containing the portal-bearing vertex were calculated.
422 Graphics were prepared using PyMOL (Schrodinger, 2015) and UCSF Chimera (Pettersen et al.,
423 2004).

424

425 **Data Availability:**

426 Maps for the UL25-Null A-capsid and the procapsid, both showing the portal vertex, were
427 deposited in the Electron Microscopy Database under accession numbers EMDB-22378 and
428 EMDB-22379, respectively.

429

430 **Acknowledgements**

431 We thank Dr. Fred L. Homa (University of Pittsburgh) for providing us with the HSV-1 UL25-Null
432 mutants and the complementary, UL25-expressing African Green Monkey cell line as well as a
433 wild type African Green Monkey cell line. We thank Dr. Jay Brown for useful discussions. This
434 work was supported by the Intramural Research Program of the National Institute for Arthritis,
435 Musculoskeletal and Skin Diseases, NIH and used the NIH Multi-Institute Cryo-EM Facility
436 (MICEF).

437

438 **Competing Interests:**

439 The authors declare no competing interests.

440

441 **References:**

442 Adelman, K., Salmon, B., & Baines, J. D. (2001). Herpes simplex virus DNA packaging sequences
443 adopt novel structures that are specifically recognized by a component of the cleavage
444 and packaging machinery. *Proc Natl Acad Sci U S A, 98*(6), 3086-3091.
445 doi:10.1073/pnas.061555698
446 Aksyuk, A. A., Newcomb, W. W., Cheng, N., Winkler, D. C., Fontana, J., Heymann, J. B., & Steven,
447 A. C. (2015). Subassemblies and asymmetry in assembly of herpes simplex virus
448 procapsid. *MBio, 6*(5), e01525-01515. doi:10.1128/mBio.01525-15
449 al-Kobaisi, M. F., Rixon, F. J., McDougall, I., & Preston, V. G. (1991). The herpes simplex virus
450 UL33 gene product is required for the assembly of full capsids. *Virology, 180*(1), 380-
451 388. doi:10.1016/0042-6822(91)90043-b
452 Baines, J. D., Poon, A. P., Rovnak, J., & Roizman, B. (1994). The herpes simplex virus 1 UL15 gene
453 encodes two proteins and is required for cleavage of genomic viral DNA. *J Virol, 68*(12),
454 8118-8124. Retrieved from https://www.ncbi.nlm.nih.gov/pubmed/7966602
455 https://jvi.asm.org/content/jvi/68/12/8118.full.pdf
456 Bauer, D. W., Huffman, J. B., Homa, F. L., & Evilevitch, A. (2013). Herpes virus genome, the
457 pressure is on. *J Am Chem Soc, 135*(30), 11216-11221. doi:10.1021/ja404008r

458 Booy, F. P., Trus, B. L., Newcomb, W. W., Brown, J. C., Conway, J. F., & Steven, A. C. (1994).
459 Finding a needle in a haystack: detection of a small protein (the 12-kDa VP26) in a large
460 complex (the 200-MDa capsid of herpes simplex virus). *Proc Natl Acad Sci U S A, 91*(12),
461 5652-5656. doi:10.1073/pnas.91.12.5652
462 Cardone, G., Winkler, D. C., Trus, B. L., Cheng, N., Heuser, J. E., Newcomb, W. W., . . . Steven, A.
463 C. (2007). Visualization of the herpes simplex virus portal in situ by cryo-electron
464 tomography. *Virology, 361*(2), 426-434. Retrieved from
465 http://www.ncbi.nlm.nih.gov/entrez/query.fcgi?cmd=Retrieve&db=PubMed&dopt=Cita
466 tion&list_uids=17188319
467 Church, G. A., & Wilson, D. W. (1997). Study of herpes simplex virus maturation during a
468 synchronous wave of assembly. *J Virol, 71*(5), 3603-3612. Retrieved from
469 https://www.ncbi.nlm.nih.gov/pubmed/9094633
470 Dai, X., & Zhou, Z. H. (2018). Structure of the herpes simplex virus 1 capsid with associated
471 tegument protein complexes. *Science, 360*(6384). doi:10.1126/science.aao7298
472 Dedeo, C. L., Cingolani, G., & Teschke, C. M. (2019). Portal Protein: The Orchestrator of Capsid
473 Assembly for the dsDNA Tailed Bacteriophages and Herpesviruses. *Annu Rev Virol*.
474 doi:10.1146/annurev-virology-092818-015819
475 Draganova, E. B., Zhang, J., Zhou, Z. H., & Heldwein, E. E. (2020). Structural basis for capsid
476 recruitment and coat formation during HSV-1 nuclear egress. *Elife, 9*.
477 doi:10.7554/eLife.56627
478 Gao, M., Matusick-Kumar, L., Hurlburt, W., DiTusa, S. F., Newcomb, W. W., Brown, J. C., . . .
479 Colonno, R. J. (1994). The protease of herpes simplex virus type 1 is essential for
480 functional capsid formation and viral growth. *J Virol, 68*(6), 3702-3712. Retrieved from
481 https://www.ncbi.nlm.nih.gov/pubmed/8189508
482 https://jvi.asm.org/content/jvi/68/6/3702.full.pdf
483 Gong, D., Dai, X., Jih, J., Liu, Y. T., Bi, G. Q., Sun, R., & Zhou, Z. H. (2019). DNA-Packing Portal and
484 Capsid-Associated Tegument Complexes in the Tumor Herpesvirus KSHV. *Cell, 178*(6),
485 1329-1343 e1312. doi:10.1016/j.cell.2019.07.035
486 Guasch, A., Pous, J., Ibarra, B., Gomis-Ruth, F. X., Valpuesta, J. M., Sousa, N., . . . Coll, M. (2002).
487 Detailed architecture of a DNA translocating machine: the high-resolution structure of
488 the bacteriophage phi29 connector particle. *J Mol Biol, 315*(4), 663-676.
489 doi:10.1006/jmbi.2001.5278
490 Heymann, J. B., Cardone, G., Winkler, D. C., & Steven, A. C. (2008). Computational resources for
491 cryo-electron tomography in Bsoft. *J Struct Biol, 161*(3), 232-242. Retrieved from
492 http://www.ncbi.nlm.nih.gov/entrez/query.fcgi?cmd=Retrieve&db=PubMed&dopt=Cita
493 tion&list_uids=17869539
494 Heymann, J. B., Cheng, N., Newcomb, W. W., Trus, B. L., Brown, J. C., & Steven, A. C. (2003).
495 Dynamics of herpes simplex virus capsid maturation visualized by time-lapse cryo-
496 electron microscopy. *Nat Struct Biol, 10*(5), 334-341. Retrieved from
497 http://www.ncbi.nlm.nih.gov/entrez/query.fcgi?cmd=Retrieve&db=PubMed&dopt=Cita
498 tion&list_uids=12704429
499 Huet, A., Makhov, A. M., Huffman, J. B., Vos, M., Homa, F. L., & Conway, J. F. (2016). Extensive
500 subunit contacts underpin herpesvirus capsid stability and interior-to-exterior allostery.
501 *Nat Struct Mol Biol*. doi:10.1038/nsmb.3212

502 Johnson, D. C., & Baines, J. D. (2011). Herpesviruses remodel host membranes for virus egress.
503 *Nat Rev Microbiol, 9*(5), 382-394. doi:10.1038/nrmicro2559
504 Liu, Y. T., Jih, J., Dai, X., Bi, G. Q., & Zhou, Z. H. (2019). Cryo-EM structures of herpes simplex
505 virus type 1 portal vertex and packaged genome. *Nature, 570*(7760), 257-261.
506 doi:10.1038/s41586-019-1248-6
507 Machon, C., Fabrega-Ferrer, M., Zhou, D., Cuervo, A., Carrascosa, J. L., Stuart, D. I., & Coll, M.
508 (2019). Atomic structure of the Epstein-Barr virus portal. *Nat Commun, 10*(1), 3891.
509 doi:10.1038/s41467-019-11706-8
510 Mastronarde, D. N. (2005). Automated electron microscope tomography using robust
511 prediction of specimen movements. *J Struct Biol, 152*(1), 36-51. Retrieved from
512 http://www.ncbi.nlm.nih.gov/entrez/query.fcgi?cmd=Retrieve&db=PubMed&dopt=Cita
513 tion&list_uids=16182563
514 McElwee, M., Vijayakrishnan, S., Rixon, F., & Bhella, D. (2018). Structure of the herpes simplex
515 virus portal-vertex. *PLoS Biol, 16*(6), e2006191. doi:10.1371/journal.pbio.2006191
516 McNab, A. R., Desai, P., Person, S., Roof, L. L., Thomsen, D. R., Newcomb, W. W., . . . Homa, F. L.
517 (1998). The product of the herpes simplex virus type 1 UL25 gene is required for
518 encapsidation but not for cleavage of replicated viral DNA. *J Virol, 72*(2), 1060-1070.
519 Retrieved from https://www.ncbi.nlm.nih.gov/pubmed/9445000
520 https://www.ncbi.nlm.nih.gov/pmc/articles/PMC124578/pdf/jv001060.pdf
521 Mettenleiter, T. C., Klupp, B. G., & Granzow, H. (2009). Herpesvirus assembly: an update. *Virus*
522 *Res, 143*(2), 222-234. doi:10.1016/j.virusres.2009.03.018
523 Mettenleiter, T. C., Muller, F., Granzow, H., & Klupp, B. G. (2013). The way out: what we know
524 and do not know about herpesvirus nuclear egress. *Cell Microbiol, 15*(2), 170-178.
525 doi:10.1111/cmi.12044
526 Newcomb, W. W., Homa, F. L., Thomsen, D. R., Booy, F. P., Trus, B. L., Steven, A. C., . . . Brown, J.
527 C. (1996). Assembly of the herpes simplex virus capsid: characterization of intermediates
528 observed during cell-free capsid formation. *J Mol Biol, 263*(3), 432-446.
529 doi:10.1006/jmbi.1996.0587
530 Newcomb, W. W., Homa, F. L., Thomsen, D. R., Trus, B. L., Cheng, N., Steven, A., . . . Brown, J. C.
531 (1999). Assembly of the herpes simplex virus procapsid from purified components and
532 identification of small complexes containing the major capsid and scaffolding proteins. *J*
533 *Virol, 73*(5), 4239-4250. Retrieved from
534 https://www.ncbi.nlm.nih.gov/pubmed/10196320
535 https://www.ncbi.nlm.nih.gov/pmc/articles/PMC104203/pdf/jv004239.pdf
536 Newcomb, W. W., Juhas, R. M., Thomsen, D. R., Homa, F. L., Burch, A. D., Weller, S. K., & Brown,
537 J. C. (2001). The UL6 gene product forms the portal for entry of DNA into the herpes
538 simplex virus capsid. *J Virol, 75*(22), 10923-10932. doi:10.1128/JVI.75.22.10923-
539 10932.2001
540 Newcomb, W. W., Trus, B. L., Cheng, N., Steven, A. C., Sheaffer, A. K., Tenney, D. J., . . . Brown, J.
541 C. (2000). Isolation of herpes simplex virus procapsids from cells infected with a
542 protease-deficient mutant virus. *J Virol, 74*(4), 1663-1673. Retrieved from
543 https://www.ncbi.nlm.nih.gov/pubmed/10644336
544 https://www.ncbi.nlm.nih.gov/pmc/articles/PMC111641/pdf/jv001663.pdf

545 Pettersen, E. F., Goddard, T. D., Huang, C. C., Couch, G. S., Greenblatt, D. M., Meng, E. C., &
546 Ferrin, T. E. (2004). UCSF Chimera--a visualization system for exploratory research and
547 analysis. *J Comput Chem, 25*(13), 1605-1612. Retrieved from
548 http://www.ncbi.nlm.nih.gov/entrez/query.fcgi?cmd=Retrieve&db=PubMed&dopt=Cita
549 tion&list_uids=15264254
550 Rochat, R. H., Liu, X., Murata, K., Nagayama, K., Rixon, F. J., & Chiu, W. (2011). Seeing the portal
551 in herpes simplex virus type 1 B capsids. *J Virol, 85*(4), 1871-1874.
552 doi:10.1128/JVI.01663-10
553 Schmid, M. F., Hecksel, C. W., Rochat, R. H., Bhella, D., Chiu, W., & Rixon, F. J. (2012). A tail-like
554 assembly at the portal vertex in intact herpes simplex type-1 virions. *PLoS Pathog, 8*(10),
555 e1002961. doi:10.1371/journal.ppat.1002961
556 Schrodinger, LLC. (2015). *The PyMOL Molecular Graphics System, Version 1.8*.
557 Sheaffer, A. K., Newcomb, W. W., Gao, M., Yu, D., Weller, S. K., Brown, J. C., & Tenney, D. J.
558 (2001). Herpes simplex virus DNA cleavage and packaging proteins associate with the
559 procapsid prior to its maturation. *J Virol, 75*(2), 687-698. doi:10.1128/JVI.75.2.687-
560 698.2001
561 Singer, G. P., Newcomb, W. W., Thomsen, D. R., Homa, F. L., & Brown, J. C. (2005). Identification
562 of a region in the herpes simplex virus scaffolding protein required for interaction with
563 the portal. *J Virol, 79*(1), 132-139. doi:79/1/132 [pii]
564 10.1128/JVI.79.1.132-139.2005
565 Trus, B. L., Booy, F. P., Newcomb, W. W., Brown, J. C., Homa, F. L., Thomsen, D. R., & Steven, A.
566 C. (1996). The herpes simplex virus procapsid: structure, conformational changes upon
567 maturation, and roles of the triplex proteins VP19c and VP23 in assembly. *J Mol Biol,*
568 *263*(3), 447-462. Retrieved from
569 http://www.ncbi.nlm.nih.gov/entrez/query.fcgi?cmd=Retrieve&db=PubMed&dopt=Cita
570 tion&list_uids=8918600
571 Trus, B. L., Cheng, N., Newcomb, W. W., Homa, F. L., Brown, J. C., & Steven, A. C. (2004).
572 Structure and polymorphism of the UL6 portal protein of herpes simplex virus type 1. *J*
573 *Virol, 78*(22), 12668-12671. doi:10.1128/JVI.78.22.12668-12671.2004
574 Trus, B. L., Homa, F. L., Booy, F. P., Newcomb, W. W., Thomsen, D. R., Cheng, N., . . . Steven, A.
575 C. (1995). Herpes simplex virus capsids assembled in insect cells infected with
576 recombinant baculoviruses: structural authenticity and localization of VP26. *J Virol,*
577 *69*(11), 7362-7366. Retrieved from https://www.ncbi.nlm.nih.gov/pubmed/7474170
578 https://jvi.asm.org/content/jvi/69/11/7362.full.pdf
579 Wang, N., Chen, W., Zhu, L., Zhu, D., Feng, R., Wang, J., . . . Wang, X. (2020). Structures of the
580 portal vertex reveal essential protein-protein interactions for Herpesvirus assembly and
581 maturation. *Protein Cell*. doi:10.1007/s13238-020-00711-z
582 White, C. A., Stow, N. D., Patel, A. H., Hughes, M., & Preston, V. G. (2003). Herpes simplex virus
583 type 1 portal protein UL6 interacts with the putative terminase subunits UL15 and UL28.
584 *J Virol, 77*(11), 6351-6358. doi:10.1128/jvi.77.11.6351-6358.2003
585 Yang, K., & Baines, J. D. (2009a). Proline and tyrosine residues in scaffold proteins of herpes
586 simplex virus 1 critical to the interaction with portal protein and its incorporation into
587 capsids. *J Virol, 83*(16), 8076-8081. doi:10.1128/JVI.00655-09

588 Yang, K., & Baines, J. D. (2009b). Tryptophan residues in the portal protein of herpes simplex
589 virus 1 critical to the interaction with scaffold proteins and incorporation of the portal
590 into capsids. *J Virol, 83*(22), 11726-11733. doi:10.1128/JVI.01463-09
591 Yang, Y., Yang, P., Wang, N., Chen, Z., Su, D., Zhou, Z. H., . . . Wang, X. (2020). Architecture of
592 the herpesvirus genome-packaging complex and implications for DNA translocation.
593 *Protein Cell*. doi:10.1007/s13238-020-00710-0
594 Yu, D., & Weller, S. K. (1998). Herpes simplex virus type 1 cleavage and packaging proteins UL15
595 and UL28 are associated with B but not C capsids during packaging. *J Virol, 72*(9), 7428-
596 7439. Retrieved from https://www.ncbi.nlm.nih.gov/pubmed/9696839
597 https://www.ncbi.nlm.nih.gov/pmc/articles/PMC109972/pdf/jv007428.pdf
598

599

Supplementary material

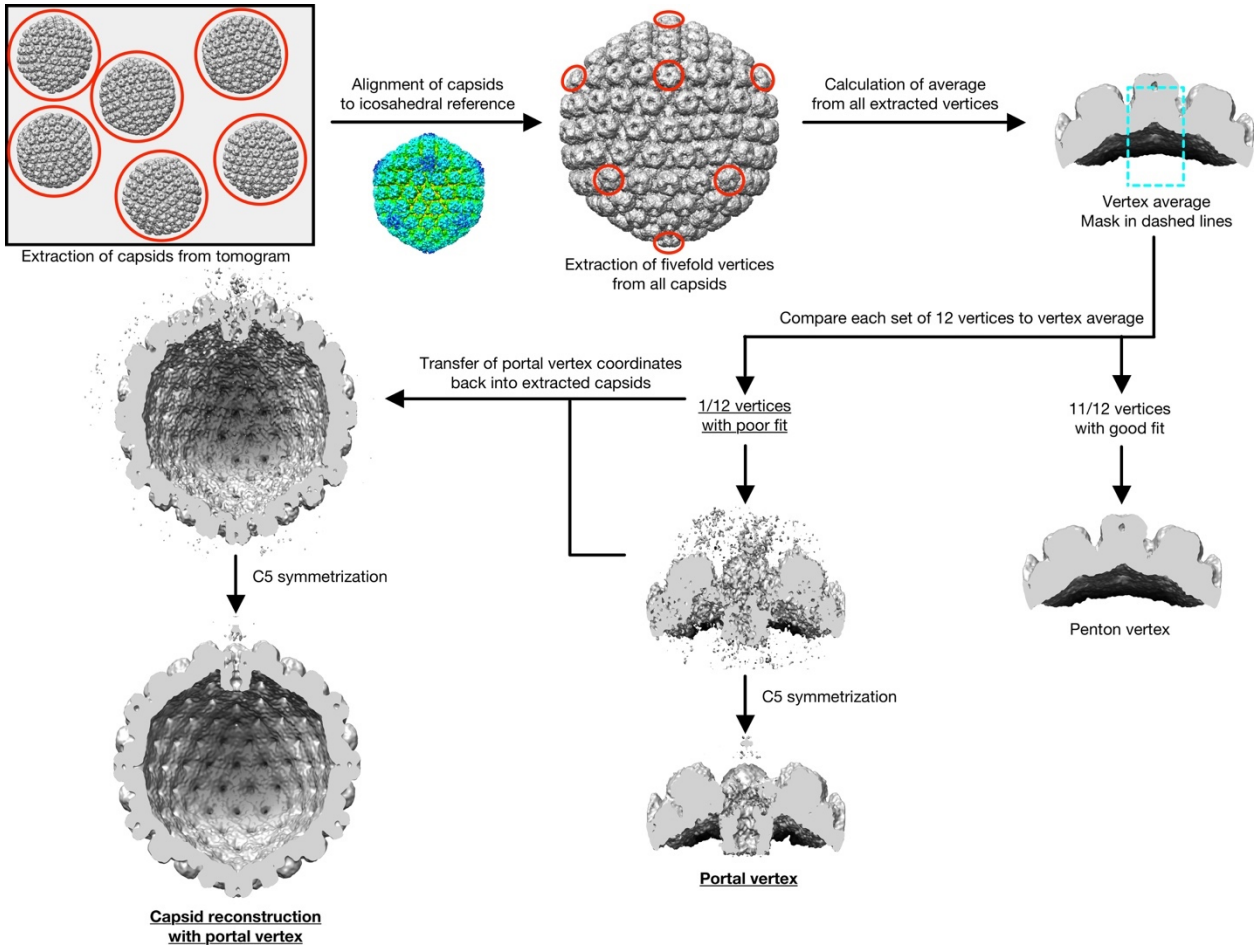

Fig. S1. General workflow used to identify and average the portal vertices. Individual particles in random orientations are extracted from tomograms and aligned with an icosahedral reference [30]. The twelve vertices of each particle were extracted, aligned, and each vertex was then compared to the average of all extracted vertices, calculating the correlation within a mask centered around the expected portal location (cyan dashed line). The vertex with the lowest correlation was taken to be the portal vertex. Its positional coordinates were then used to transform that whole capsid into an orientation that placed the portal vertex on the same five-fold axis to allow C5 symmetrization.

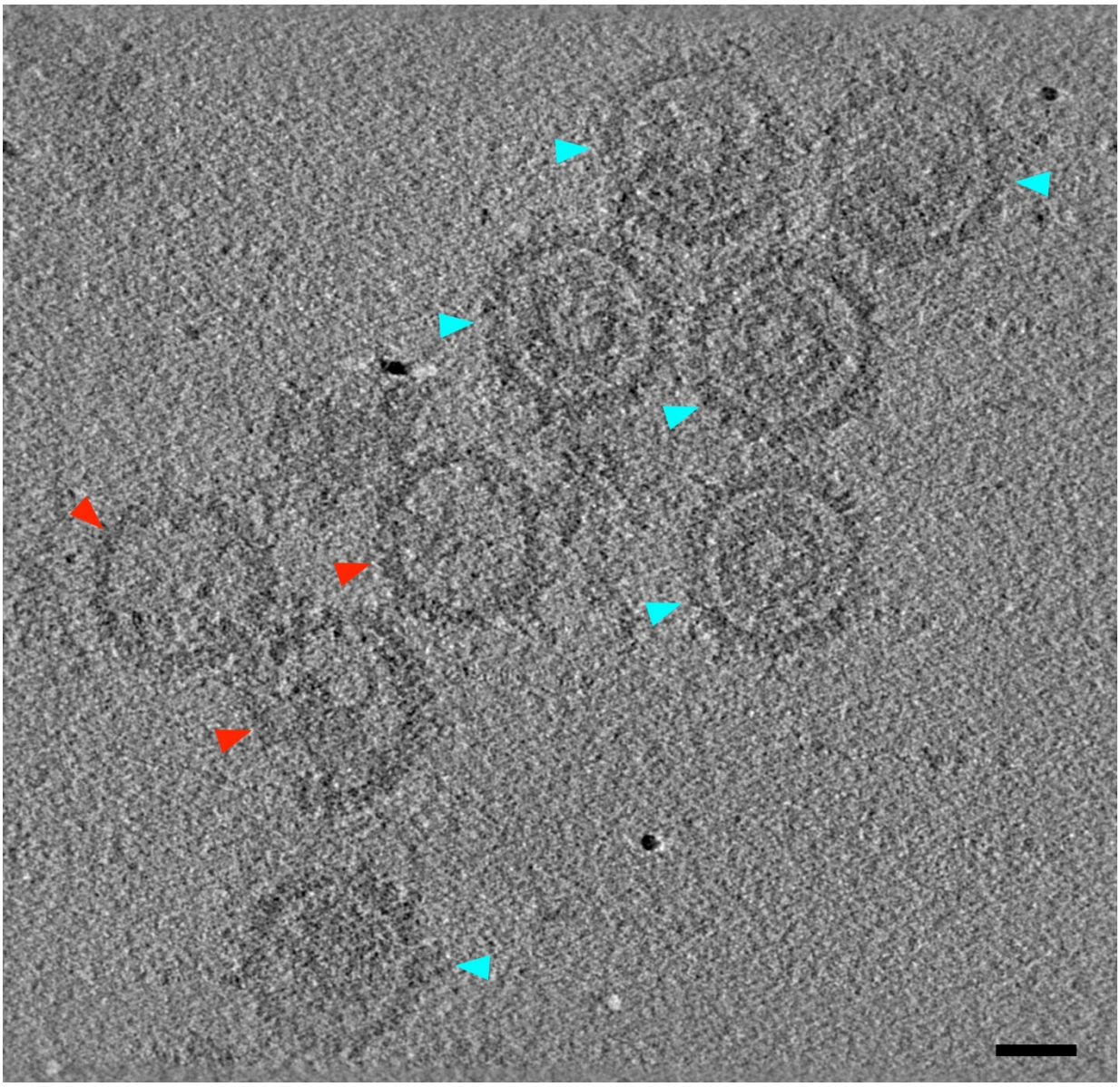

Fig. S2. Central slice of a tomographic reconstruction of procapsids. Some particles contained visibly degraded scaffold or showed imperfections (red arrowheads) and were excluded from further processing. We took care to include only particles that were separated, spherical, and had a visibly intact scaffold (turquoise arrowheads). The procapsid at the bottom of this field is located at a different height making it appear smaller than the other particles. Scale bar, 500 Å.